Available online at www.sciencedirect.com
SCIENCE DIRECT®
Journal of Nuclear Materials 352 (2006) 116–125
journal of nuclear materials
www.elsevier.com/locate/jnucmat

Crack resistance curves determination of tube cladding material

J. Bertsch *, W. Hoffelner

Paul Scherrer Institut, CH-5232 Villigen PSI, Switzerland

Abstract

Zirconium based alloys have been in use as fuel cladding material in light water reactors since many years. As claddings change their mechanical properties during service, it is essential for the assessment of mechanical integrity to provide parameters for potential rupture behaviour. Usually, fracture mechanics parameters like the fracture toughness K_{IC} or, for high plastic strains, the J-integral based elastic–plastic fracture toughness J_{IC} are employed. In claddings with a very small wall thickness the determination of toughness needs the extension of the J-concept beyond limits of standards. In the paper a new method based on the traditional J approach is presented. Crack resistance curves (J–R curves) were created for unirradiated thin walled Zircaloy-4 and aluminium cladding tube pieces at room temperature using the single sample method. The procedure of creating sharp fatigue starter cracks with respect to optical recording was optimized. It is shown that the chosen test method is appropriate for the determination of complete J–R curves including the values $J_{0.2}$ (J at 0.2 mm crack length), J_m (J corresponding to the maximum load) and the slope of the curve.

PACS: 62.20.Mk; 81.40.Lm; 81.40.Np; 81.70.Bt

1. Introduction

A manufactured component is, a-priori, expected to be defect-free. But in practice any material of a component may contain flaws or flaws can be created during special operational conditions. The question is whether such a flaw can expand into a crack and whether this crack is going to propagate. Especially for Zircaloy components in a nuclear environment eventually the question of safe operation or handling of the component arises. For normal operational conditions in a nuclear power plant axial split of Zircaloy cladding tubes or the behaviour of cracks in other thin walled components as spacers/grids may be a concern. For the period after service, during transportation (vibrations, shocks), intermediate dry storage (delayed hydride cracking, stress corrosion cracking) or final storage [1] fracture toughness properties of fuel cladding can become relevant.

The use of fracture mechanics technology for reactor Zircaloy issues has been limited in the past. This is partly due to a lack of regulatory emphasis on cladding failure as a safety issue [2] and to the fact that much of the standard fracture mechanics methodology does not apply to standard light water reactor (LWR) bundle component geometries. The use of fracture mechanics to predict the behaviour of cracks or defects is increasing. Papers at recent international conferences have illustrated fracture

* Corresponding author. Tel.: +41 56 310 4173; fax: +41 56 310 2203.
E-mail address: johannes.bertsch@psi.ch (J. Bertsch).

0022-3115/$ - see front matter © 2006 Elsevier B.V. All rights reserved.
doi:10.1016/j.jnucmat.2006.02.045

mechanics techniques for analysing crack propagation in failed Zircaloy tubing [3–5]. And for many years, leak-before-break criteria and critical crack lengths in CANDU-type reactor (CANada Deuterium Uranium) pressure tubes have been analysed using fracture toughness methodology [6].

The strict methodology of LEFM usually does not apply to geometries (particularly thicknesses) of interest to reactor components. The plastic zone sizes of zirconium alloys are too large. For example: In order to satisfy the criteria of ASTM Standard E399 [7] for valid fracture toughness K_{IC} determination for a only roughly expected $K_{IC} = 55$ MPa $m^{1/2}$ and a yield stress of 600 MPa for irradiated Zircaloy at 573 K, the thickness of the tested samples must exceed a value of about 21 mm. This is many times the thickness of cladding, grid, channel, etc., components. For unirradiated Zircaloy the required thickness would be even larger.

To accommodate soft material the *J*-integral is frequently applied. As commonly used, '*J*' is related to the amount of work (dissipative energy, both elastic and plastic) per unit crack surface area required to extend a crack. But, it is strictly valid only in the case where the crack grows in an elastic material. Its use, however, has been extended [8,9] to include elastic–plastic materials like Zircaloy or for small radioactive samples of nuclear application relevant steels [10]. But even the less stringent size requirements for the applicability of the *J*-integral are not met theoretically by thin walled claddings. This work attempts to find a *J*-type approach to define mechanical quantities of claddings which allow a prediction of the fracture behaviour of cladding material with different toughness. In analogy to the conventional fracture mechanics approach such quantities should be as far as possible independent from specimen geometry to allow their application to components and realistic crack geometries.

2. Experimental

2.1. Material

The experiments were carried out with samples fabricated from the aluminium alloy Al-7050 and cold-worked stress relieved (SRA) Zircaloy-4. Cold-worked SRA Zircaloy was selected because it shows a lower tendency to very early crack blunting compared to re-crystallized Zircaloy. The aluminium alloy which exhibits significant lower fracture toughness was chosen because of comparison reasons.

2.2. Sample geometry

Our approach was based on the following criteria:

- In order to have a well defined starting point we have chosen a specimen geometry, which basis is well characterized under valid stress intensity factor *K* and *J* conditions.
- With respect to later testing of service exposed cladding material the geometry should also allow easy manipulator handling.
- All parameters reported for established *K* and *J* testing should be measurable.

Fracture mechanics samples can be of bending type or of tension type. Typical bending type samples are the compact tension (CT) specimen and the single edge notched (SEN) bending sample [11]. Well known tension type samples are the single or double edge notched tension (SENT, DENT) samples or the centre notched panel (CN). Because of our approach criteria, basically a pipe type tensile version was chosen.

Fig. 1 shows the tested different notched samples and the influence of their geometries and pre-cracking on the failure behaviour. To use an optimal sample form for generating well defined starter cracks by fatigue and to have a situation as close as possible to a potential real crack in a cladding tube, various tube sample geometries and the geometries' influence on the pre-cracking procedure were tested. The wall thickness of the samples *B* is 0.6 mm, the width *W* is 12.5 mm and the notch length *l* is dependent on the cutting process. The two edge notches on the front side of the DENT-like ring sample are cut with a wire saw, the holes of the samples which we designate CHT (central hole tension) and CLHT (central long hole tension) are drilled and the notch of the CNT (central notch tension) sample is cut by spark erosion. All hole and notch types are situated at the sample front side. The notch lengths and sizes respectively are about 0.8–1.0 mm (DENT), 1.1 mm in diameter (CHT), 1.2 mm × 3.2 mm (CLHT) and 0.4 mm × 1.8 mm (CNT).

2.3. Experimental equipment

The samples were tested on an electro-mechanical Schenck testing machine at room temperature in air. We used the 'one sample method'. Crack lengths and strain were recorded optically with a

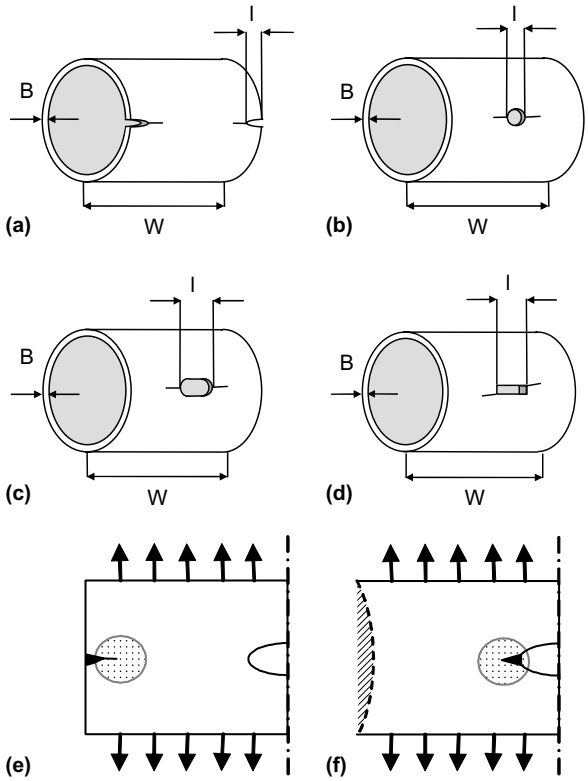

Fig. 1. Tested sample geometries for pre-cracking optimization ($B = 0.6$ mm, $W = 12.5$ mm, l is dependent on the cutting process) and influence of pre-cracking on the crack development during tensile testing (plastic regime): (a) double edge notched, tensile (DENT), (b) central hole, tensile (CHT), (c) central long hole, tensile (CLHT), (d) central notch, tensile (CNT), (e) stress concentration at crack tip after fatigue, (f) stress concentration at central notch (no prior fatigue).

digital camera. Pictures were taken at given time intervals.

The gripping sections to apply a mechanical load to the sample are shown in Fig. 2. The two segments on the top fit the inner diameter of the sample and can be slipped into it. The grips are machined as counterparts of the segments. This assembly allows the application of tangentially oriented stresses to the cladding sample. The question of possible bending of the sections was checked. Using the above mentioned optical measuring device no bending was detected.

2.4. Pre-cracking and crack development

The notched sample is fatigue loaded until a fatigue crack starts to grow. The stress amplitude of the fatigue loading is in the elastic regime (up to 30% of the yield stress). The following cracking behaviour in dependency on sample (notch) type could be identified:

- In the case of fatigue in the elastic regime (pre-cracking), the cracks start always at the outer side(s) of the sample, independent on the existence of a central notch.
- Performing a tensile test with prior fatigue, i.e. fatigue cracks are at the outer sides, the failure starts at the outer edges (respectively outer fatigue cracks), even if the sample is centrally notched.
- Making a tensile test with non-fatigued, centrally notched specimens (rapidly going to the plastic regime), the failure begins at the central notch.
- If there are several fatigue cracks or notches with fatigue cracks, failure always occurs at the weakest link, i.e. at the place with the highest stress intensity factor.
- As the CNT sample – cut by spark erosion in a rectangular form – exhibits distinct corners in the notch (stress concentrators), cracks often occur asymmetrically or are not in the sample mid plane, i.e. not orthogonal to the load line (see Fig. 1(d)). Therefore this sample type could be classified as inappropriate for our test procedure.

The explanation for the different behaviour can be found in the changed specimen response in the elastic and plastic case. At the edges and near the opening segments, which fit into the sample, stress peaks arise (this is also endorsed by the FEM calculations which are described below). In the elastic regime, the stress peaks make the fatigue cracks occur at the outer sides independently of the presence of a central notch. If the fatigue is followed by a tensile test (plastic regime), the stress concentration at the crack tip is the relevant driving force and the prior fatigue crack extends (see Fig. 1(e)).

In the case of a tensile test without prior fatigue (plastic regime), the failure of a central notched specimen begins at the highest stress concentration, which can be found in the radius of the notch. Without a pre-crack, the transition from elasticity to plasticity inverts the stress distribution between sample outer side and central notch. The reason for the stress inversion is in our opinion a very small yielding at the outer side. This yielding in form of a minimal bowing is illustrated in Fig. 1(f). The geometry change by the yielding at the outer sides leads

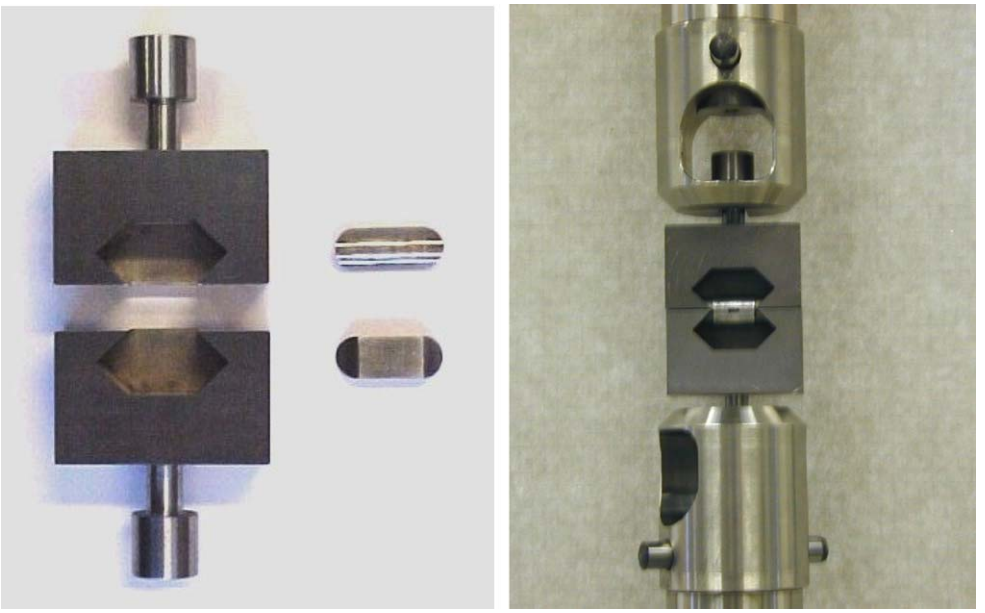

Fig. 2. Gripping section and sample placed in the machine.

to a lowering of the initially higher stresses at the outer edges relative to the central part. The failure finally begins at the central notch. The conclusion of the selection procedure is that the DENT sample geometry is the most adapted for the chosen test setup.

2.5. DENT sample and FEM modelling

The question was how the pre-cracked DENT-like ring sample would react under tension. The interest was focused on the difference of stress and strain behaviour of the notched front side and the back side. Therefore we let calculate the deformation and stresses for several initial fatigue crack lengths (Marti-Technology AG, F. Gazeau, Emmenbrücke, Switzerland). Some results are shown in Fig. 3. It became clear that the relative deformation is concentrated in the notched region (Fig. 3(a)) and the highest stresses are in front of the crack tips (Fig. 3(b)). With the asymmetric sample weakening – notches only on one side – failure always happens on the weak side by elastic–plastic deformation. The deformation on the opposite side is only elastic. The FEM calculations confirmed our decision to choose the DENT-like ring sample for further testing. As the relevant sample deformation happens on the front side, crack propagation and failure are always accessible for optical recording.

3. Evaluation of data

3.1. Tensile testing

The sequence of Fig. 4 shows the different stages of the development of a crack during stable crack growth conditions. The starter notches and the fatigue cracks appear dark. The cracks propagating under unidirectional load appear white (see indication by arrows in Fig. 4). Crack propagation and strain in the sample's mid-plane were measured electronically on the taken pictures. To be sure to obtain the relevant local strain at the mid plane of the samples, the strain was determined by measuring the opening of the notches, i.e. the vertical distance between the borders of the notches at each side. In Fig. 5(a) an example of load displacement curve is shown for each Zircaloy and aluminium. The open symbols signify the opening of the right and left notch, respectively. The full symbols show the average. The opening is not absolutely symmetrical at each time. But it can be recognized that one notch does not overrule the other one all the time. This means there is no self sustaining, increasing instability, i.e. tilting of the sample. The system is self adjusting to a certain grade. Additionally we verified that no bending of the gripping sections affected the strain measurement. No bending was measurable.

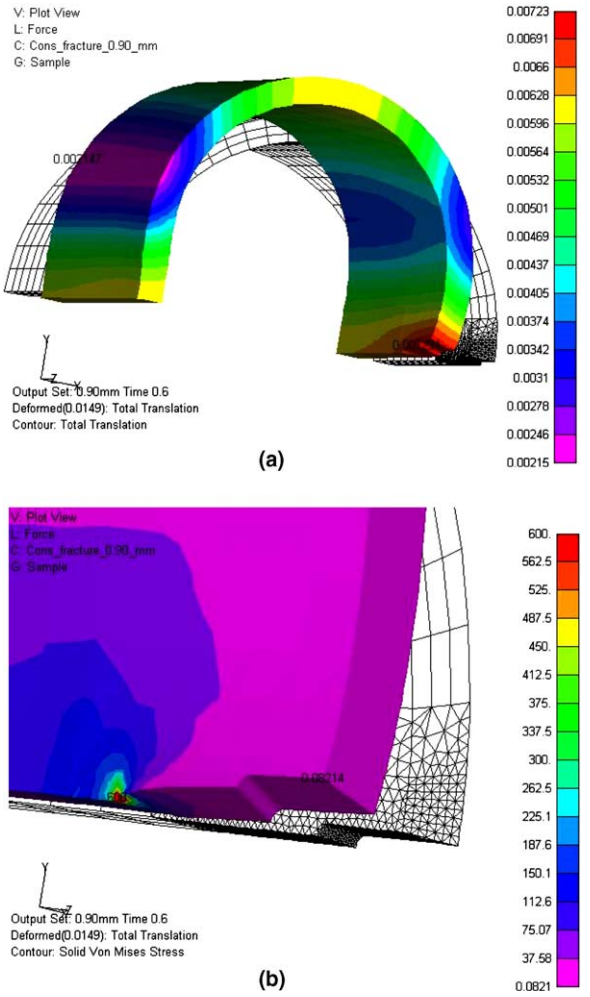

Fig. 3. Tensile FEM calculations for 0.9 mm crack length and load at beginning plastic deformation (calculations by Marti-Technology AG, F. Gazeau, Emmenbrücke, Switzerland): (a) Total translation (concentration of the displacement in the notched region) and (b) Von Mises stresses (plasticity concentrated at the crack tip).

Typical load–displacement curves for aluminium and Zircaloy are summarized in Fig. 5(b). The data show a relatively high scatter. Reasons might be the slight differences in the fatigue crack lengths and increasing importance of the material microstructure (grains) with decreasing specimen size.

3.2. Friction correction and J determination

Because of its asymmetric form the sample makes a very small movement in the gripping when being tested (see Fig. 6). This leads to energy dissipation by friction. For the calculation of the J, which is energy per crack prolongation, the amount of friction energy has to be taken into account.

As shown in the FEM calculations, the plastic deformation happens at the notched front side of the sample. This additional deformation at the front – at the backside is only elastic deformation – is responsible for the gliding of the sample over the two segments of the gripping system. For the calculation of the friction energy, the normal (orthogonal) force, the friction displacement and the friction coefficient are needed. The normal force can be obtained from the load measurements; the friction relevant displacement is derived from the plastic part of movement. Even though the important role of friction for Zircaloy tube testing has been recognized [12,13], friction relevant references are very rare. They concern the friction between ceramic pellets, UO_2 or Al_2O_3, and unirradiated Zircaloy [14,15]. For the friction coefficient between Zircaloy and steel we used the averaged value from [16]. But it is clear that the friction coefficient rests dependent on the surface quality of the sliding partners. In reality the friction between cladding and pellet can strongly change during reactor operation and increasing burn-up. Starting from an energy balance with the total energy E_{tot}, plastic energy E_{pl}, elastic energy E_{el} and friction energy E_{fr} (see Eq. (1)), a load correction $F_{\mathrm{corr},i}$ for each moment i can be calculated incrementally (Eq. (2)):

$$E_{\mathrm{tot}} = E_{\mathrm{pl}} + E_{\mathrm{el}} + E_{\mathrm{fr}}, \tag{1}$$

$$F_{\mathrm{corr},i} = F_{\mathrm{uncorr},i} \cdot \frac{D_i}{k \cdot 0.5 \cdot D_{\mathrm{pl},i} + D_i}. \tag{2}$$

$F_{\mathrm{uncorr},i}$ is the force given by the machine at the moment i, D_i and $D_{\mathrm{pl},i}$ are the incremental total and plastic displacements, k is the friction coefficient. The factor 0.5 emerges because only the half of the plastic displacement has to be taken into account. The reason for that is the plasticity contribution to the displacement on both sides.

The J-integral was determined according to the ASTM standard E 1820 [17]. It has to be stated that the procedure was very similar to the standard but can naturally not exactly follow it, because of (a) the special sample geometry and (b) using the friction model.

J consists of an elastic and plastic component, $J = J_{\mathrm{el}} + J_{\mathrm{pl}}$; whereas the elastic part is computed from the elastic stress intensity factor K as

$$J_{\mathrm{el}} = \frac{K^2}{E'}, \tag{3}$$

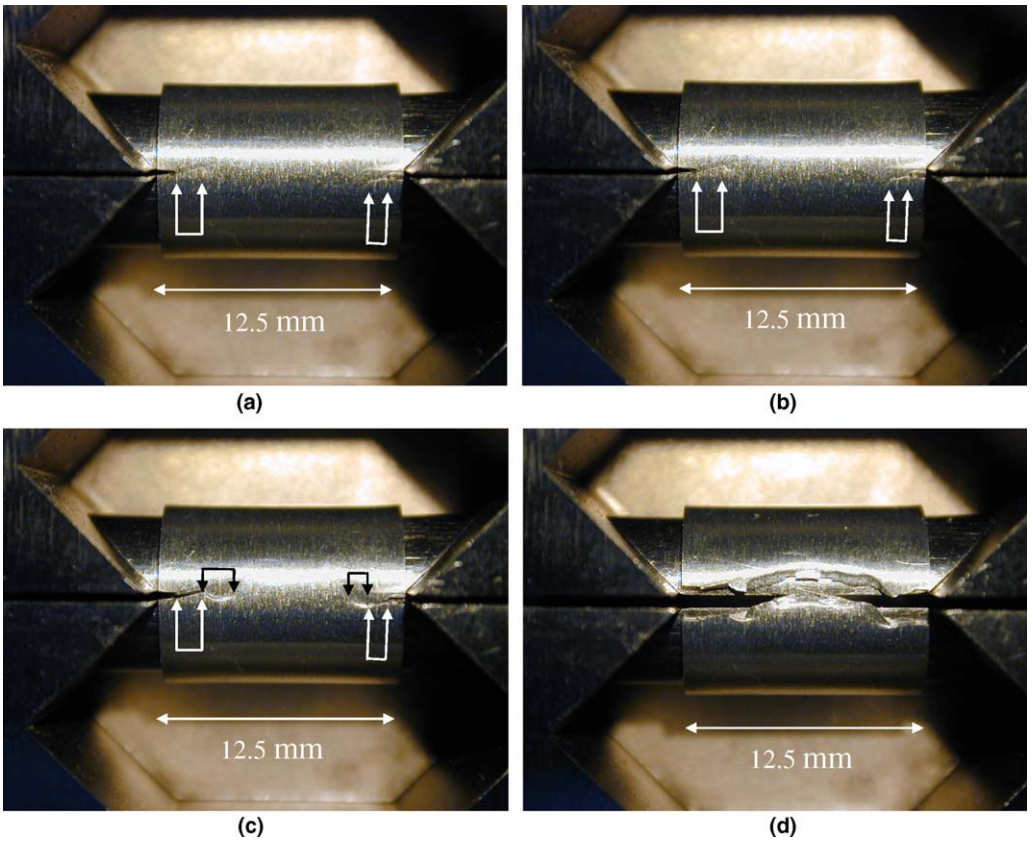

Fig. 4. Crack growth under tensile conditions: (a) just before starting of stable crack growth, only fatigue cracks are visible (white arrows), (b) just after stable crack growth started (mainly white crack contrast), (c) appearance of cracks just before final rupture (black arrows indicate growing crack), (d) appearance of the cladding after final rupture.

where $E' = E$ for plane stress and $E' = E/(1 - v^2)$ for plane strain with Young's modulus E and Poisson's ratio v. Because of the thickness of the sample we consider the situation as plane stress and therefore used $E' = E = 100$ GPa for Zircaloy and $E' = E = 70$ GPa for aluminium.

The stress intensity factor K is related to the stress intensity function $f(a/W)$ by the equation

$$K = \frac{P}{B} \cdot \sqrt{\frac{2}{W}} \cdot f\left(\frac{a}{W}\right), \tag{4}$$

where P is the applied load for one side of the sample (half of the complete load), B the specimen wall thickness, W the specimen width, a = crack length and $f(a/W)$ = dimensionless stress intensity function.

The plastic J-integral $J_{\mathrm{pl},i}$ at the moment i is evaluated with a recurrence formula, being calculated incrementally and taking into account the continuous crack growth, i.e. continuous geometry change during loading

$$J_{\mathrm{pl},i} = J_{\mathrm{pl},i-1} \cdot \left(1 - \frac{\Delta a_{i-1}}{b_{i-1}}\right) + \frac{A_i}{B b_{i-1}} \cdot \left(1 - \frac{\Delta a_i}{b_{i-1}}\right) \tag{5}$$

where A_i is the area under the plastic part of the load deflection curve, a_i the crack length, Δa_i the difference between a_i and a_{i-1}, b_i is the difference between W and a_i and B is the specimen wall thickness.

4. J–R curves and results

The J–R curves for Zircaloy and aluminium shown in Fig. 7 are constructed according to the above mentioned standard. The slope of the four additional lines in the plot is $M \cdot \sigma_y$. M is set two and σ_y is the effective yield strength, i.e. the mean value of yield strength and tensile strength. For σ_y we have taken 625 MPa for Zircaloy and 475 MPa for aluminium. The J–R curves are fitted with exponential functions, determined by using the J-values

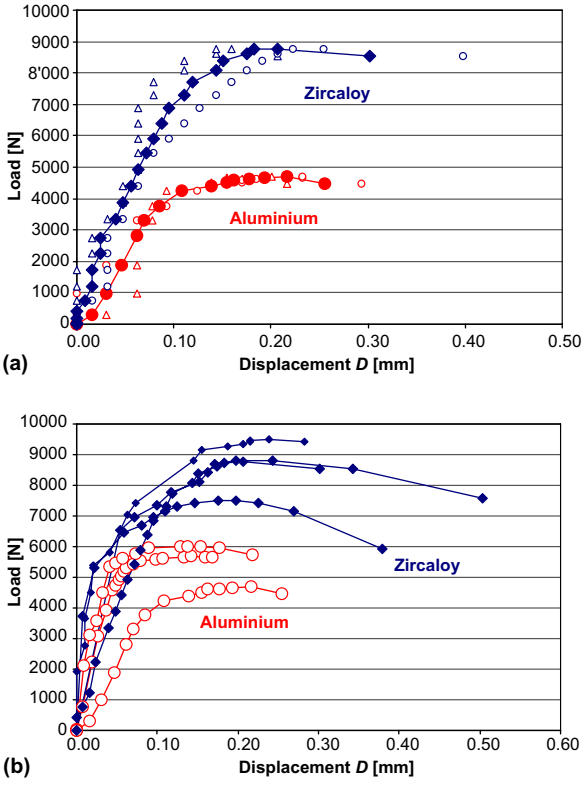

Fig. 5. Load–displacement curves: (a) Comparison – opening of left notch (△), right notch (○) and mean values (closed symbols); (b) Zircaloy and for comparison reasons aluminium.

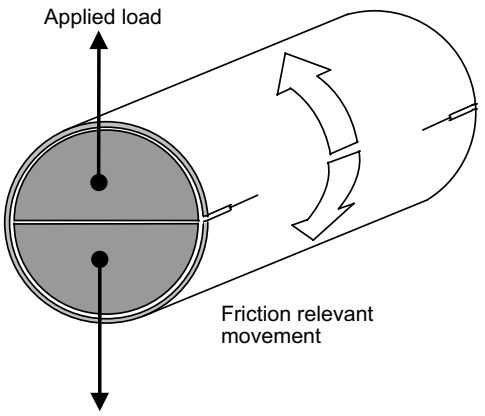

Fig. 6. Sample movement at beginning plasticity (arrows indicate direction); sliding of the sample on the gripping sections.

between the two exclusion lines starting at 0.15 and 1.5 mm, respectively. Characteristic for the crack resistance are the following values (results are summarized in Table 1 for Zircaloy and Table 2 for aluminium):

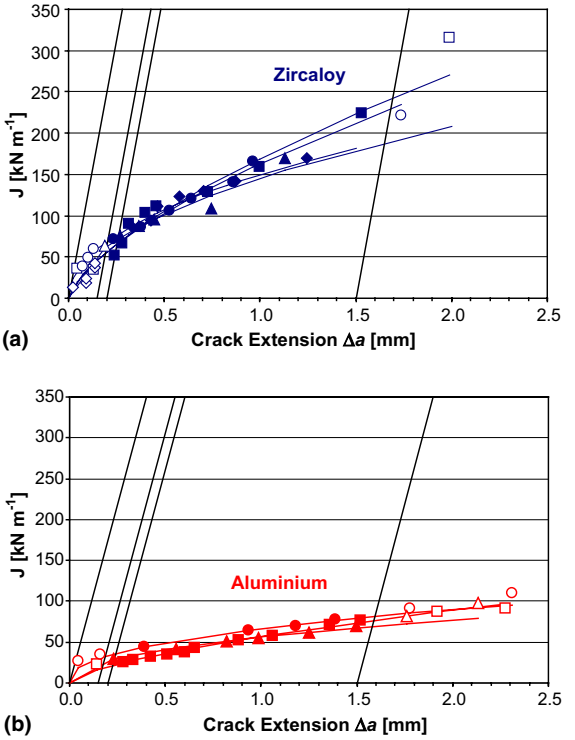

Fig. 7. *J–R* curves (points with open symbols do not contribute to the fit functions): (a) Zircaloy (four samples) and (b) aluminium (three samples).

- $J_{0.2}$, which is determined by the intersection of the 0.2 mm offset line (the third line in the plot) with the fit function. This value is characteristic for beginning crack propagation.
- J_m corresponds to the maximum load in the load displacement curve. In our opinion this value strongly depends on the sample geometry.
- The slope dJ/da of the J–R curve also characterizes the toughness of the material. A higher slope means higher resistance against the propagation of an existing crack at given crack length. The slope decreases with increasing crack prolongation; in Tables 1 and 2 we have listed the slopes at $J_{0.2}$.

Table 1
Test results Zircaloy

Sample no.	$J_{0.2}$ (kN m^{-1})	J_m (kN m^{-1})	dJ/da at $J = J_{0.2}$ (MPa)
1	66.1	99.2	178.8
2	71.4	75.3	145.6
3	65.3	106.2	172.2
4	79.1	94.1	143.9
Average	70.5 ± 6.4	93.7 ± 13.2	160.1 ± 18.0

Table 2
Test results aluminium

Sample no.	$J_{0.2}$ (kN m^{-1})	J_m (kN m^{-1})	dJ/da at $J = J_{0.2}$ (MPa)
1	21.1	34.8	62.2
2	36.1	44.7	64.9
3	28.8	55.4	57.3
Average	28.7 ± 7.5	45.0 ± 10.3	61.5 ± 3.9

Some SEM analyses of the crack morphologies have been performed. The crack propagation at the beginning of the tensile testing starts orthogonally to the applied load. It has to be mentioned that after some time the crack tilts into a more shear mode direction. Typically this has not yet taken place at $J_{0.2}$. A quantitative analysis of the crack morphologies has not yet been done.

5. Discussion

A differentiation between the tougher Zircaloy and the less tough aluminium for $J_{0.2}$, J_m and the slope of the J–R curve can clearly be displayed. A result of this type was expected with respect to the load–displacement curves, where higher final forces and displacements were necessary for Zircaloy. The '$J_{0.2}$ fracture toughness' for Zircaloy is in average more than the double compared to aluminium. Even with a very small non-standard sample wall thickness the chosen test procedure delivers results in a consistent way. The scatter bands are reasonably small. They are much smaller as compared to the load displacement curves. This shows the principal aptitude of the J determining procedure and, especially, of the friction correction.

Our results fit well in the range of literature data, as can be seen in Fig. 8. Fig. 8(a) shows a comparison of J values and Fig. 8(b) a comparison of K values, whereas – for better comparability – our $J_{0.2}$ and J_m results were converted to K values according to $K = (J \cdot E')^{1/2}$, with $E' = 100$ GPa.

Grigoriev et al. [4] reported J values for cold-worked and annealed Zircaloy-2, hydrided and irradiated and tested at different temperatures. Grigoriev used cut cladding tube pieces in a pin load test. For evaluation of our results we have taken the results of the cold-worked, unirradiated and non-hydrided samples tested a room temperature (see Fig. 8(a)). The properties of the cold-worked samples should come closest to the properties of our material. Grigoriev's J values are higher than our $J_{0.2}$ values, rather being in the range of the J_m values. This can simply be explained by the measurement procedure. Grigoriev determined J at maximum load of the load-displacement curve, corresponding to our J_m. A significant difference of values of cold-worked Zircaloy-2 and our cold-worked stress-relieved annealed Zircaloy-4 cannot be deduced from the comparison.

Bertolino et al. published in a series of articles [18–20] several fracture toughness values of unirradiated Zircaloy-4. Plate material was hot rolled, annealed and then cold rolled before cutting into samples. In case of [18] and [19], small CT like samples were used, in case of [20] small single edge notched bending (SENB) samples were tested in a SEM, observing crack initiation and propagation in situ. The focus of these articles is on fracture toughness properties at different hydrogen contents and temperatures. The values in Fig. 8(a) are taken from [18] and concern tests at room temperature and correspond to crack initiation. Thus, they can be compared with our $J_{0.2}$ values. Most of the

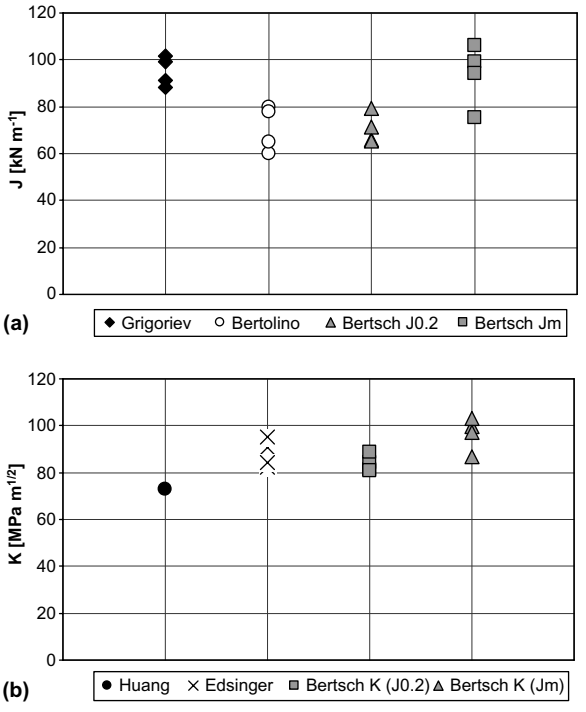

Fig. 8. Comparison of published fracture toughness data for Zircaloy (details see text): (a) J values (Grigoriev: [4], Bertolino: [18], Bertsch: $J_{0.2}$ and J_m of this paper) and (b) K values (Huang: [22], Edsinger: [3], Bertsch: $J_{0.2}$ and J_m of this paper converted into K).

samples were hydrogen loaded. The highest J value coming from this paper and which is displayed in Fig. 8(a) is around 80 kN m^{-1}. It corresponds to a very low hydrogen content of approximately 30–40 ppm. The other displayed values belong to higher but still low hydrogen contents of approximately 100–120 ppm. In the mentioned paper, there is one data point for none-hydrogen loaded samples with a very high value at above 300 kN m^{-1} (not shown in Fig. 8(a)). The data in [19] indicate similar characteristics. Material with a very low content of 10 ppm H delivers a $J_{0.2}$ value of approximately 300 kN m^{-1}, whereas a slightly higher H content of already 50 ppm lets the $J_{0.2}$ drop strongly down to approximately 100 kN m^{-1}. The differences between the curves for low (50 ppm H) and higher hydrogen contents are relatively small. The testing of the SENB samples in a SEM [20] reveals for low H contents (approximately 30–50 ppm) $J_{0.2}$ values somewhat above 100 kN m^{-1}. Because of very few non-hydrogen loaded values, in our opinion the most reasonable comparison with Bertolino's data can be done by taking the low hydrogen loaded results.

Dubey et al. [21] determined J–R curves for small curved CT specimen fabricated out of Zircaloy-2 pressure tubes for Indian pressurized heavy water reactors (PHWR); the results are not shown in Fig. 8. The tube manufacturing steps comprise extrusion and two stage cold pilgerings with an intermediate annealing. The J_{IC} value for the unirradiated material without hydrogen charging (10–15 ppm H) is high, i.e. 275 kN m^{-1}. But also the slope of the J–R curve ($dJ/da = 207$ MPa) is significantly higher than our average slope at $J_{0.2}$ ($dJ/da = 160$ MPa). The reasons for the higher values are not clear, but might be found in the tubes manufacturing process and the curved sample geometry.

Huang [22] determined the fracture toughness of Zircaloy-2 CT samples cut from reactor pressure tubes. Crack propagation was measured with the potential drop method and crack initiation was attributed to the first potential drop. The so determined fracture toughness can be compared to our $J_{0.2}$ respectively the corresponding K values. In Fig. 8(b) the result for the unirradiated sample tested at room temperature is shown. The reason for Huang's somewhat lower K value might be its determination at the very first crack initiation (potential drop) whereas we used $J_{0.2}$, i.e. when crack propagation has already started.

Edsinger et al. [3] describe the so called Vallecitos Embedded Charpy (VEC) test. A half of a notched and pre-cracked tube section is embedded in jackets and then loaded like in a 3-point-bend fracture toughness test. Edsinger used different reactor irradiated material. For the comparison we have taken the data of non-irradiated, cold-worked Zircaloy-2 which was tested at room temperature (see Fig. 8(b)). The determined K values correspond to maximum load, i.e. the values can be compared with our J_m results, being converted to K values. Edsinger's results are quite well in line with our data, but slightly lower than our J_m values. This might be attributed to the stress-relieving annealing of our samples.

It can be summarized that the published data and our results match well, although different test methods were used. Discrepancies can mostly be explained by differences in the analysis procedure or materials properties. The applied new test method seems to deliver reasonable and comparable test results. However it is clear that, due to the limitations of sample thickness, it is not possible to obtain a standard fracture toughness value that is a true material property.

6. Conclusions and outlook

A new fracture mechanics J-type approach for the determination of fracture toughness of thin walled claddings was developed, using a tension loaded modified DENT-like ring sample. The method delivers whole crack resistance (J–R) curves including the characteristic values $J_{0.2}$ (J at starting crack of 0.2 mm length), J_m (J corresponding to maximum load in the load-displacement curve) and eventually the slope of the J–R curve. It provides a quantitative relationship between a flaw of given size (fretting defect, production defect, hydride lens, etc.) and the tolerable loads and it can therefore be linked with safety considerations. Future work will be aimed at improving and expanding the method:

- Better understanding of the friction between the cladding and the test gripping sections. Friction plays an important role for real cladding – especially of high burn-up fuel – concerning energy deposition during failure. Friction can be investigated by using different surface finish or application of different lubrications between sample and gripping sections.

- Applying the method to further thin walled Zircaloy components to better elucidate the local elastic–plastic behaviour, additionally using finite element modelling.
- Application to higher, reactor relevant temperatures, other environments and other loading conditions (creep, fatigue, etc.).
- Another experimental challenge will be to apply this method to service exposed cladding materials from nuclear power plants and to determine toughness values of differently hydrided materials and different burn-ups.

Acknowledgements

The authors wish to thank Mr Ph. Meyer for supporting the mechanical testing, Mr Roland Bruetsch for his help on SEM observations and Ph. Spätig (CRPP, EPF Lausanne) for making available the Schenck testing machine.

References

[1] K.S. Chan, Y. Lee, Nucl. Eng. Des. 201 (2000) 209.
[2] U.S. Nuclear Regulatory Commission Standard Review Plan, NUREG-0800, NRC, 2, July 1981.
[3] K. Edsinger, J.H. Davies, R.B. Adamson, in: G.P. Sabol, G.D. Moan (Eds.), Zirconium in the Nuclear Industry: Twelfth International Symposium, ASTM STP 1354, West Conshohocken, 2000, p. 316.
[4] V. Grigoriev, B. Josefsson, B. Rosborg, in: E.R. Bradley, G.P. Sabol (Eds.), Zirconium in the Nuclear Industry: Eleventh International Symposium, ASTM STP 1295, 1996, p. 431.
[5] Y.R. Rashid, C. Lemaignan, A. Strasser, Evaluation of Fracture Initiation and Extension in Fuel Cladding, ANS Int'l Topical Meeting LWR Fuel Performance, Park City, April 10–13, 2000.
[6] P.H. Davies, R.S.W. Shewfelt, in: G.P. Sabol, G.D. Moan (Eds.) Zirconium in the Nuclear Industry: Twelfth International Symposium, ASTM STP 1354, West Conshohocken, 2000, p. 356.
[7] ASTM E 399, Standard Test Method for Linear-Elastic Plane-Strain Fracture Toughness K_{IC} of Metallic Materials, ASTM international.
[8] N.E. Dowling, Mechanical Behavior of Materials, second ed., Prentice-Hall, Inc, 1999, ISBN -0-13-905720-X.
[9] G.C. Sih, in: R.P. Wei, R.P. Gangloff (Eds.) Fracture Mechanics in Two Decades (20th Symposium), ASTM STP 1020, Philadelphia, 1989, p. 9.
[10] K. Machida, M. Kikuchi, Int. J. Pres. Ves. Pip. 63 (1995) 9.
[11] T.L. Anderson, Fracture Mechanics – Fundamentals and Applications, second ed., CRC, 1994, ISBN 0-8493-4260-0.
[12] R.S. Daum, S. Majumdar, H. Tsai, T. Bray, D.A. Koss, A.T. Motta, M.C. Billone, in: M.A. Sokolov, J.D. Landes, G.E. Lucas (Eds.), Small Specimen Test Techniques: Fourth Volume, ASTM STP 1418, West Conshohocken, 2002, p. 195.
[13] S. Arsene, J. Bai, J. Test. Eval. 24 (1996) 386.
[14] J.C. Wood, B.A. Surette, I. Aitchison, J. Nucl. Mater. 88 (1980) 81.
[15] N. Nakatsuka, J. Nucl. Mater. 96 (1981) 205.
[16] B.C. d'Agraives, J. Toornvliet, Application of a Non-dynamometric Method to the Measurement of the Coefficient of Static Friction in Cold and Hot Water Between Stainless Steel and Two Alloys of zirconium, EUR 5604 f, JNRC Ispra, 1977.
[17] ASTM E 1820-01, Standard Test Method for Measurement of Fracture Toughness, ASTM international.
[18] G. Bertolino, G. Meyer, J.P. Ipiña, J. Alloys Comp. 330–332 (2002) 408.
[19] G. Bertolino, G. Meyer, J.P. Ipiña, J. Nucl. Mater. 320 (2003) 272.
[20] G. Bertolino, G. Meyer, J.P. Ipiña, J. Nucl. Mater. 322 (2003) 57.
[21] J.S. Dubey, S.L. Wadekar, R.N. Singh, T.K. Sinha, J.K. Chakravartty, J. Nucl. Mater. 264 (1999) 20.
[22] F.H. Huang, J. Nucl. Mater. 207 (1993) 103.